Using WCP-OFDM Signals with Time-Frequency Localized Pulses for Radar Sensing

Damien Roque and Stéphanie Bidon
Institut Supérieur de l'Aéronautique et de l'Espace (ISAE-SUPAERO), Université de Toulouse, 31055 Toulouse, FRANCE
Email: {damien.roque,stephanie.bidon}@isae-supaero.fr

***Abstract*—In this paper performance of a symbol-based WCP-OFDM radar estimation algorithm is studied. Particularly, benefits of using orthogonal time-frequency localized pulses rather than biorthogonal rectangular pulses (traditionally used in CP-OFDM receiver) is investigated in presence of white Gaussian noise. Numerical examples show that the former provide better dynamic range and tolerance to Doppler for short ranges.**

***Index Terms*—Radar, multicarrier, short-length filters, non-rectangular pulses, ambiguity function.**

I. Introduction

Communication and radar capabilities are both required in various applications (*e.g.*, transportation, autonomous systems). To save RF resources, several authors have thus suggested the use of a common waveform able to jointly transmit information while sensing the environment [1]–[5].

In particular in [2]–[4], cyclic prefix orthogonal frequency-division multiplexing (CP-OFDM) shows interesting capabilities to reconcile both features. Therein, a 3-stage radar signal processing is described as follows: 1) linear estimation of the symbols; 2) data symbols removal; 3) bi-dimensional discrete Fourier transform (DFT) to recover the radar range-Doppler map.

However, this algorithm is limited to low-velocity scenarios due to the poor frequency localization of rectangular pulses used in CP-OFDM [6]. Additionally, CP removal at the radar receiver penalizes the dynamic range of the system.

In this paper we extend the radar signal processing of [2]–[4] to weighted cyclic prefix (WCP)-OFDM waveform. The latter is a generalization of CP-OFDM that allows non-rectangular short-length pulses to be used while preserving perfect symbol reconstruction and low-complexity implementation. WCP-OFDM pulses have been designed in [7] and characterized for data transmission over time-frequency selective channels in [8]. Numerical results are then provided to illustrate the potential interest to use time-frequency localized (TFL) pulses for short range applications like in automotive radar.

II. System model

Herein we recall the symbol-based radar signal processing of [2]–[4], initially described for CP-OFDM, while extending it to WCP-OFDM [8]. To that end, we introduce explicitly the pulse shapes $(g[k], \check{g}[k])$ used on transmit and receive, respectively. The radar-communication transmitter, the radar propagation channel and the radar receiver are represented in Fig. 1.

A. Transmitter: WCP-OFDM waveform

We consider a WCP-OFDM waveform with M subcarriers and K blocks. The baseband output of the discrete-time multicarrier transmitter is [9]

$$s[k] = \sum_{m=0}^{M-1} \sum_{n=0}^{K-1} c_{m,n} g[k - nN] e^{j2\pi \frac{m}{M} k}, \quad k \in \boldsymbol{Z} \qquad (1)$$

where $\{c_{m,n}\}_{(m,n)\in \boldsymbol{I}}$ is a sequence of complex symbols to transmit with $\boldsymbol{I} = \{0, \dots, M-1\} \times \{0, \dots, K-1\}$ and $g[k]$ is the pulse shape. $1/M$ and N represent (normalized) elementary symbol spacing in frequency and time, respectively. Let denote T_s the sampling time associated with the index k. Hence, from a radar point of view, the traditional communication waveform (1) is a continuous waveform with K sweeps, a period of repetition equal to NT_s (leading thus to N range gates) and a non-synthetic bandwidth equal to $B = 1/T_s$. The ambiguous range and velocity are given respectively by $R_a = cNT_s/2$ and $v_a = c/(2f_cNT_s)$ with c the speed of light and f_c the carrier frequency. Finally, we recall that the range resolution is defined by $\delta_R = c/(2B)$.

B. Channel: a single point target

Let us then consider a single target characterized by a complex amplitude b_0, a radial velocity v_0 and a round-trip delay τ_0. We assume that the latter is a multiple of the sampling period T_s so that $\tau_0 = l_0 T_s$ where l_0 denotes the target's range gate. In the remaining, a narrowband scenario is considered in the sense that the compression/dilatation due to the Doppler effect applies only to the carrier signal and not to the complex envelope (1). This is tantamount to neglecting the range migration of all targets during the whole K sweeps, namely $v_0 NT_s K \ll \delta_R$. In that case, the received signal boils down to

$$r[k] = b_0 e^{j2\pi\nu_0 kT_s} s[k - l_0] + n[k] \qquad (2)$$

where $n[k]$ is a circular Gaussian noise with zero mean and variance σ_n^2 and $\nu_0 = 2v_0 f_c/c$ is the target Doppler frequency.

C. Radar receiver

1) Following the path of [2]–[4], a linear estimation of the symbols is first performed by the radar receiver thanks to a pulse shape $\check{g}[k]$. It consists of a series of correlations between

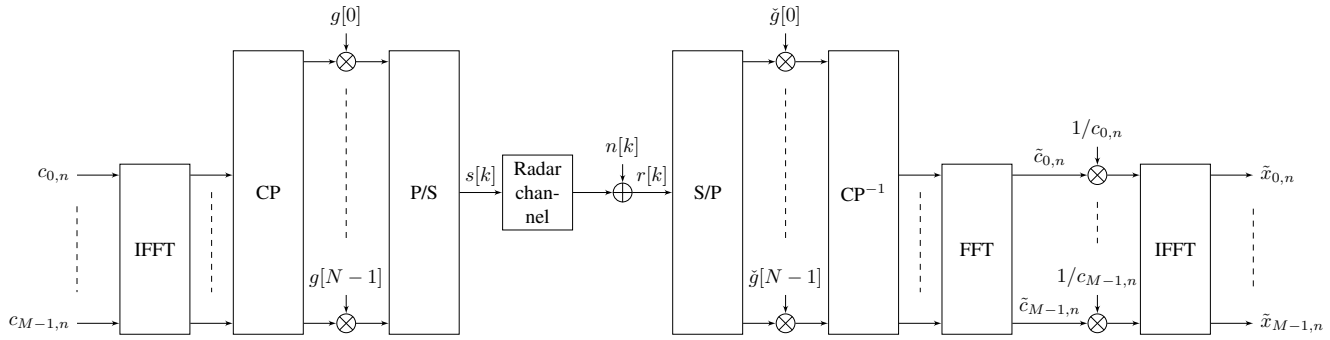

Fig. 1. Flowchart of WCP-OFDM system: radcom-transmitter, radar channel, radar receiver.

the received signal (2) and the received pulse shape shifted in frequency and time, *i.e.*,

$$\tilde{c}_{p,q} = \sum_{k\in\boldsymbol{Z}} r[k]\check{g}[k-qN]e^{-j2\pi\frac{p}{M}k}, \quad (p,q)\in\boldsymbol{I}. \tag{3}$$

This operation corresponds actually to the first stage of a conventional linear multicarrier receiver. Using the received signal model (2) and assuming that the target's velocity is much less than the ambiguous velocity, *i.e.*, $v_0 \ll v_a$, the $c_{p,q}$'s can be written after some manipulations as

$$\begin{aligned}\tilde{c}_{p,q} = b_0 \sum_{m=0}^{M-1}\sum_{n=0}^{K-1} c_{m,n}e^{-j2\pi\frac{m}{M}l_0}e^{j2\pi\left[\nu_0 T_s+\frac{m-p}{M}\right]qN} \\ \times A_{\check{g},g}\left((n-q)N+l_0, \frac{(m-p)}{M}+\nu_0 T_s\right) + n_{p,q}\end{aligned} \tag{4}$$

with the cross-ambiguity function and the noise term

$$\begin{aligned}A_{\check{g},g}(l,f) &= \sum_{k\in\boldsymbol{Z}} g[k-l]\check{g}[k]e^{j2\pi fk} \\ n_{p,q} &= \sum_{k\in\boldsymbol{Z}} n[k]\check{g}[k-qN]e^{-j2\pi\frac{p}{M}k}.\end{aligned} \tag{5}$$

In (5), l and f represent the range gate index and the normalized Doppler frequency, respectively. In this work, we focus on WCP-OFDM waveform which implies

i) positive CP length:

$$N - M \geq 0$$

ii) short length pulses:

$$g[k] = \check{g}[k] = 0 \quad \text{for} \quad k \notin \{0,\ldots,N-1\}$$

iii) pulse shapes with perfect symbol reconstruction:

$$A_{\check{g},g}((n-q)N,(m-p)/M) = \delta_{m,p}\delta_{n,q}$$

with δ the Kronecker symbol.

In search of a low-complexity radar receiver, the waveform is assumed to be range-Doppler tolerant, *i.e.*,

$$A_{\check{g},g}\left((n-q)N+l_0, \frac{(m-p)}{M}+\nu_0 T_s\right) \approx \delta_{m,p}\delta_{n,q} \tag{6}$$

where $\approx$ means "approximately proportional to", so that (4) becomes

$$\tilde{c}_{p,q} \approx b_0\, c_{p,q}e^{j2\pi\nu_0 NT_s q}e^{-j2\pi\frac{l_0}{M}p} + n_{p,q}, \quad (p,q)\in\boldsymbol{I}. \tag{7}$$

In (7) we recognize the same expression of the estimated symbols $\tilde{c}_{p,q}$ as that of [2]–[4]. This suggests to extend the rest of the CP-OFDM radar processing described therein to the more general case of WCP-OFDM waveform, *viz.*,

2) symbols removal (assumed known at the radar receiver): $\{\bar{c}_{p,q} = \tilde{c}_{p,q}/c_{p,q}\}_{(p,q)\in\boldsymbol{I}}$;
3) bi-dimensional DFT on $\{\bar{c}_{p,q}\}_{(p,q)\in\boldsymbol{I}}$ to obtain the range-Doppler map $\{\tilde{x}_{p,q}\}_{(p,q)\in\boldsymbol{I}}$ of the target scene.

III. Numerical simulations

A. Pulse shape

Prior to examining the performance of the proposed radar receiver, we focus on the characteristics of both pulse shapes used later in the simulations. We consider first the conventional rectangular pulses used in CP-OFDM, *i.e.*, for $k \in \{0,\ldots,N-1\}$,

$$g^{\text{CP}}[k] \propto 1 \quad \text{and} \quad \check{g}^{\text{CP}}[k] \quad \propto \begin{cases}1 & \text{if } k \geq N-M \\ 0 & \text{otherwise}\end{cases} \tag{8}$$

where $\propto$ means proportional to. We explain in the next section how to choose both constants of proportionality involved in (8). CP pulses were studied in [2]–[4] and serve us here as a reference point. The actual pulses of interest are TFL pulses as described in [7]. Their analytical expression is more complex and can be found in the *op-cited* reference [7]. Unlike CP pulses, TFL pulses are identical on transmit and receive, *i.e.*, $g^{\text{TFL}} = \check{g}^{\text{TFL}}$. Both CP- and TFL-pulses are represented in time and frequency domains in Fig. 2. One can indeed appreciate the improved localization of TFL pulses over CP pulses especially for high N/M ratio. This view is reinforced by depicting the cross-ambiguity function (5) for each type of pulses (Fig. 3).

B. Performance of the proposed radar receiver

Herein we compare the performance of the radar receiver of Section II for both CP- and TFL-pulses. Numerical values

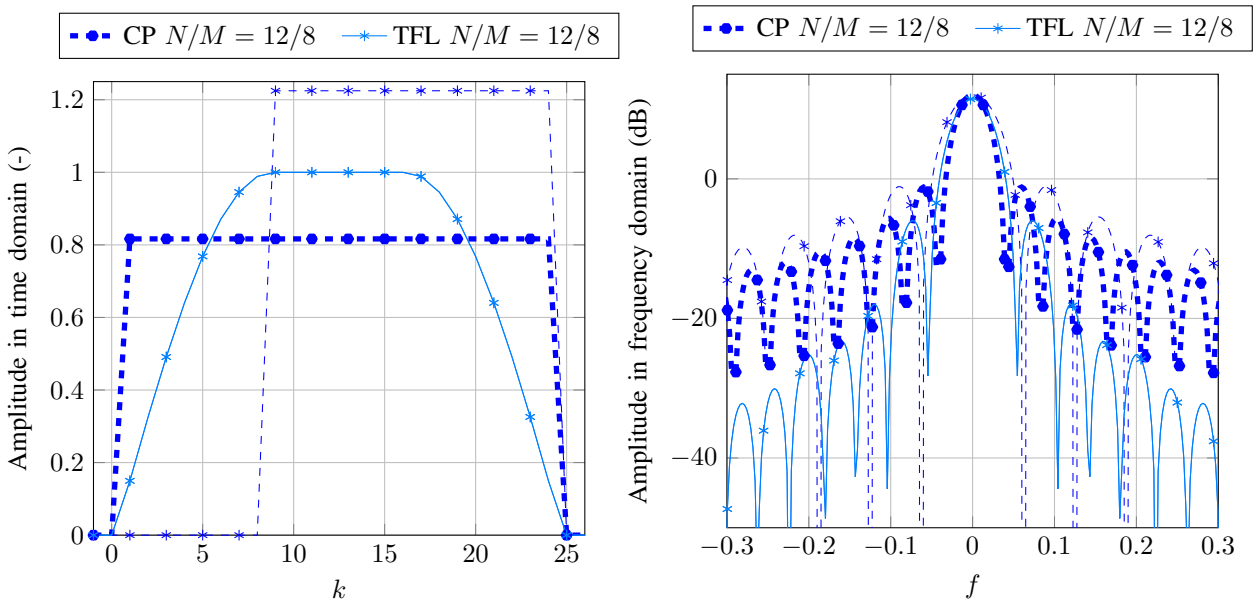

(a) Time domain representation with $N/M = 12/8$

(b) Frequency domain representation with $N/M = 12/8$

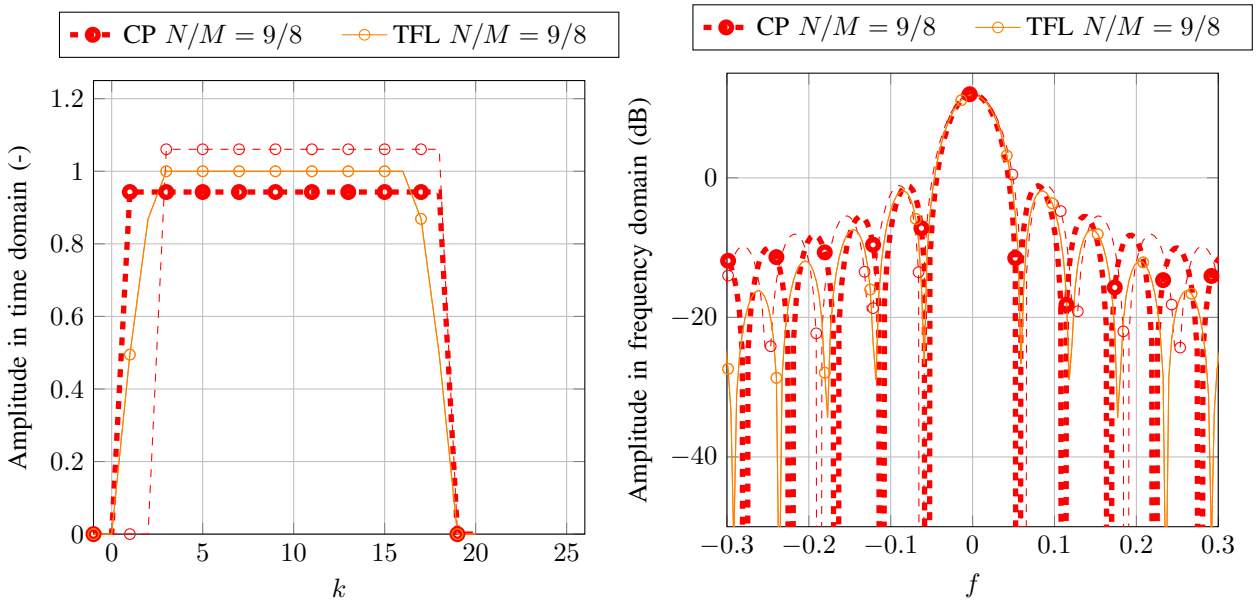

(c) Time domain representation with $N/M = 9/8$

(d) Frequency domain representation with $N/M = 9/8$

Fig. 2. CP- and TFL-pulses on transmit and receive in the time and frequency domains. CP-pulses on receive (g^{CP} thin line) are shorter than that on transmit ($\check{g}^{\mathrm{CP}}$ thick line). TFL-pulses are identical on transmit and receive, *i.e.*, $g^{\mathrm{TFL}} = \check{g}^{\mathrm{TFL}}$. $M = 16$. Time domain: (a) $N/M = 12/8$ (c) $N/M = 9/8$. Frequency domain: (b) $N/M = 12/8$ (d) $N/M = 9/8$.

used in the simulations are partly inspired from the automotive radar framework of [4]. A single target scenario is generated according to (2) where the white noise power is set to $\sigma_n^2 = 0$ dB. For a fair comparison, we ensure that the transmitted energy remains identical for both pulses by choosing an identical norm for the transmitted pulse. We set arbitrarily $\sum_k g^2[k] = M$. Note that once the amplitude of g is fixed that of $\check{g}$ is completely determined by the condition of perfect symbol reconstruction [8, Eq.(6)]. To fix then the target's amplitude b_0 in the simulations, let consider temporarily a target with null range and velocity. In that case, the approximation (6) is exact so that the post-processing signal-to-noise ratio (SNR) is shown to be

$$\mathrm{SNR} = \mathbb{E}\{|b_0|^2\} \frac{MK}{\sigma_n^2 \sum_k \check{g}^2[k]}$$

where symbols with unit variance are assumed. In what follows, the amplitude b_0 is chosen to have a target's post-processing SNR equal to 20 dB for the TFL pulses. Recall

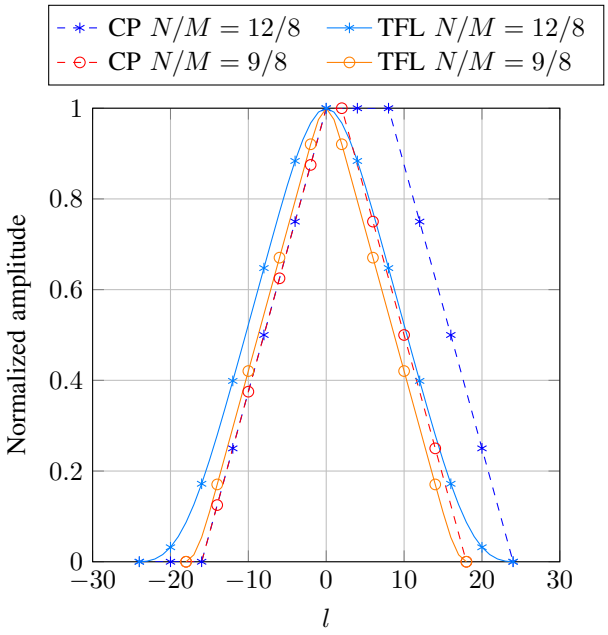

(a) Cross-ambiguity function for $f = 0$: $|A_{\check{g}g}(l, 0)|$

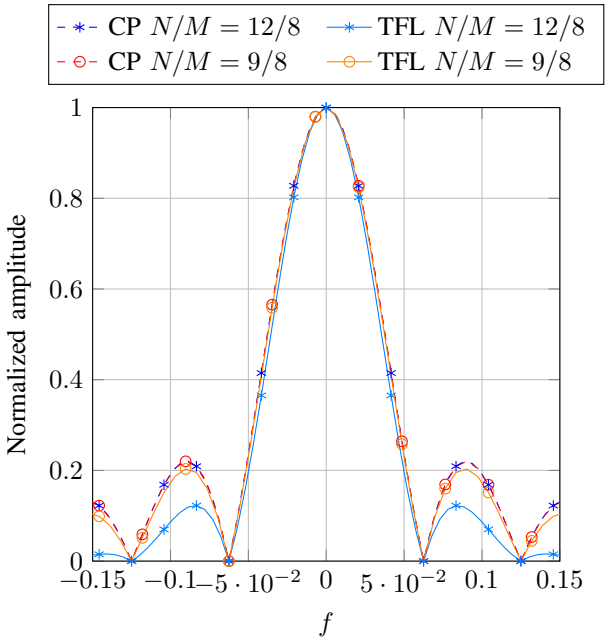

(b) Cross-ambiguity function for $l = 0$: $|A_{\check{g}g}(0, f)|$

Fig. 3. Cross-ambiguity function of $(g^{\mathrm{CP}}[k], \check{g}^{\mathrm{CP}}[k])$ and $(g^{\mathrm{TFL}}[k], \check{g}^{\mathrm{TFL}}[k])$ pulses with $M = 16$.

that this post-processing SNR is purely theoretical since in practice the target has nonzero range and/or velocity.

We evaluate numerically the SNR loss caused by the approximation (6) when either the velocity or the range is not null. In that case, mismatch between the received target echo and the pulse shape $\check{g}[k]$ may result in an additional interference component that diminishes the target peak level while increasing the interference level. These phenomena can be seen in the range-Doppler maps depicted in Fig. 4 and seem to be more accentuated for CP pulses.

To quantify more precisely these effects, we display in Fig. 5 the measured dynamic range defined as the ratio between the target peak and the average noise plus interference floor. The following should be noted.

- At null range and velocity, expected SNRs are both recovered. Unlike TFL pulses that implement a true matched filter, CP-OFDM naturally endures an integration loss of N/M due to the cyclic prefix (8).
- At null velocity, performance degrades i) continuously with the target range for TFL pulses ii) abruptly after the cyclic prefix range gate $N - M$ in CP-OFDM. At short range, TFL pulses outperform that of CP and are more robust for large N/M since the approximation (6) is then more accurate (Fig. 3a).
- At null range, the dynamic range decreases with the target velocity in both cases. Nonetheless, well frequency-localized pulses yield better tolerance to Doppler. Especially at high N/M, sidelobes of the TFL cross-ambiguity function are lower causing less subcarrier interference (Fig. 3b).

IV. Conclusion

In this paper, an OFDM waveform used traditionally in communications has been considered to implement a radar detection receiver. Particularly, we focused on the WCP-OFDM class that entails the celebrated CP-OFDM waveform using rectangular pulses as well as a class of waveform using the so called TFL pulses. The radar signal processing proposed corresponds to an extension of a previously described receiver suited only for CP pulses. The algorithm consists of three main stages: linear estimation of the symbols as done conventionally in a communication receiver followed by removal of the known symbols and finally a coherent integration leading to the conventional range-Doppler map. The proposed estimation scheme relies on the assumption of a range-Doppler tolerant waveform enabling low-computational operations. Nonetheless, in practice, the latter approximation actually induces losses particularly at high range and/or velocity. The reason of the discrepancy is twofold: loss on the target peak resulting in an increase of the ambient noise. These losses are assessed via numerical simulations while estimating the peak-to-ambient-noise ratio. In a nutshell, at short range TFL pulses lead to better dynamic range and are more tolerant to Doppler especially when their time-frequency localization, driven by the ratio N/M, augments. Hence, TFL pulses are better suited for short-range applications. An interesting continuation of this work lies in the derivation of approximate closed-form expression of the additive ambient noise power due to the target self-interference phenomenon.

References

[1] X. Chen, X. Wang, S. Xu, and J. Zhang, "A novel radar waveform compatible with communication," in *Computational Problem-Solving (ICCP), 2011 International Conference on*, Oct 2011, pp. 177–181.

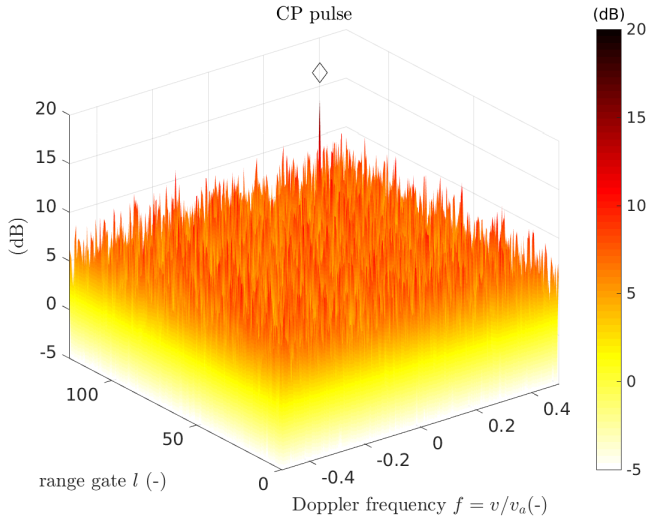

(a) Range-Doppler map with CP-pulses

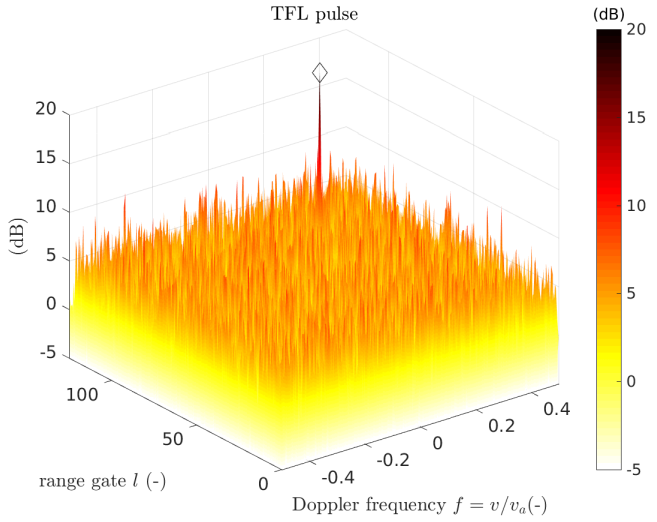

(b) Range-Doppler map with TFL-pulses

Fig. 4. Range-Doppler map for (a) CP pulses (b) TFL pulses. $f_c = 24$ GHz, $1/T_s = 93.1$ MHz, $M = 1024$, $K = 256$, $N/M = 12/8$, [ambiguous velocity $v_a \approx 379$ m/s, range resolution $\delta_R \approx 1.6$ m, cyclic prefix $N-M = 512$ range gates $= 825$ m], $\sigma_n^2 = 1$, b_0 such that $\text{SNR}^{\text{TFL}} = 20$ dB for a theoretical target at null range and velocity. Diamond markers represent true location of target.

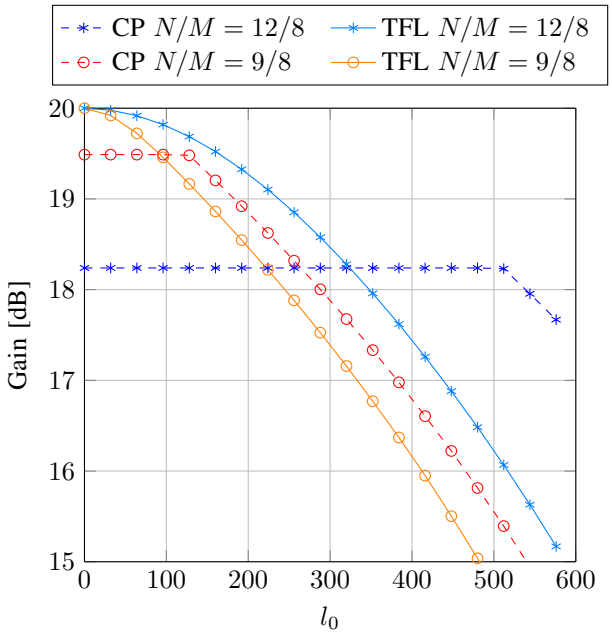

(a) Dynamic range for $v_0 = 0$

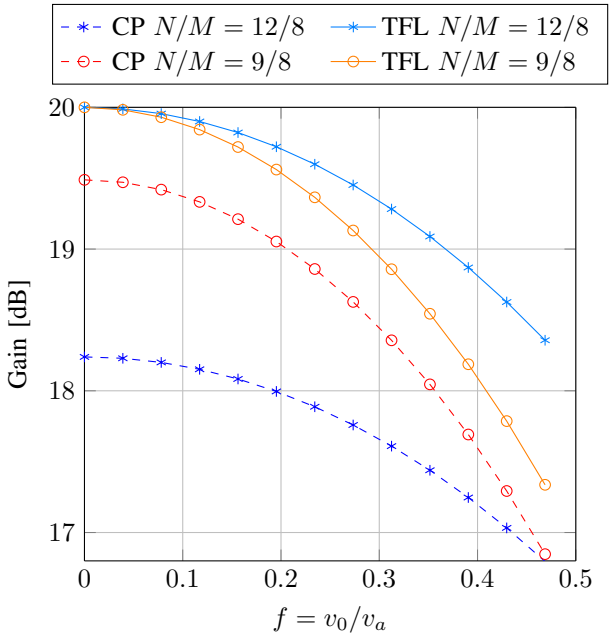

(b) Dynamic range for $l_0 = 0$

Fig. 5. Dynamic range as a function of the target (a) range (b) velocity. $f_c = 24$ GHz, $1/T_s = 93.1$ MHz, $M = 1024$, $K = 256$, [ambiguous velocity $v_a \approx 379$ m/s, range resolution $\delta_R \approx 1.6$ m, cyclic prefix $N - M$ range gates], $\sigma_n^2 = 1$, b_0 such that $\text{SNR}^{\text{TFL}} = 20$ dB for a theoretical target at null range and velocity.

[2] C. Sturm, T. Zwick, and W. Wiesbeck, "An OFDM system concept for joint radar and communications operations," in *Vehicular Technology Conference, 2009. VTC Spring 2009. IEEE 69th*, April 2009, pp. 1–5.

[3] M. Braun, C. Sturm, and F. K. Jondral, "Maximum likelihood speed and distance estimation for OFDM radar," in *Radar Conference, 2010 IEEE*, May 2010, pp. 256–261.

[4] C. Sturm and W. Wiesbeck, "Waveform design and signal processing aspects for fusion of wireless communications and radar sensing," *Proceedings of the IEEE*, vol. 99, no. 7, pp. 1236–1259, July 2011.

[5] S. Koslowski, M. Braun, and F. K. Jondral, "Using filter bank multicarrier signals for radar imaging," in *Position, Location and Navigation Symposium - PLANS 2014, 2014 IEEE/ION*, May 2014, pp. 152–157.

[6] G. E. A. Franken, H. Nikookar, and P. V. Genderen, "Doppler tolerance of OFDM-coded radar signals," in *Radar Conference, 2006. EuRAD 2006. 3rd European*, Sept 2006, pp. 108–111.

[7] D. Pinchon and P. Siohan, "Closed-form expressions of optimal short PR FMT prototype filters," in *Proc. IEEE Global Telecommunications Conf. GLOBECOM '11*, 2011.

[8] D. Roque and C. Siclet, "Performances of weighted cyclic prefix OFDM with low-complexity equalization," *IEEE Commun. Lett.*, vol. 17, no. 3, pp. 439–442, 2013.

[9] C. Siclet, P. Siohan, and D. Pinchon, "Oversampled orthogonal and biorthogonal multicarrier modulations with perfect reconstruction," in *Digital Signal Processing, 2002. DSP 2002. 2002 14th International Conference on*, vol. 2, 2002, pp. 647–650 vol.2.